Scaling of light scattered from fractal aggregates at resonance

Guillermo P. Ortiz[1,2,*] and W. Luis Mochán[2,†]
[1]*Facultad de Ciencias, Universidad Autónoma del Estado de Morelos, Av. Universidad s/n, 62210 Cuernavaca, Morelos, Mexico*
[2]*Centro de Ciencias Físicas, Universidad Nacional Autónoma de México, Apartado Postal 48-3, 62251 Cuernavaca, Morelos, Mexico*
(Received 19 December 2001; revised manuscript received 2 January 2003; published 16 May 2003)

Due to the scale invariance of fractal aggregates, light scattered from them often decays as a power of the scattering wave vector. The exponent in this power law has been usually interpreted as the geometrical fractal dimension. However, the validity of this interpretation is questionable for frequencies close to the resonances of the system, for which multiple scattering becomes important. In this work we calculate the dipole moments optically induced in fractal aggregates and the corresponding self-consistent field, as well as the electromagnetic normal modes. To this end, we develop a multiresolution hierarchical representation of the aggregate that allows the study of large systems taking fully into account the long range of the interactions. We analyze the scaling properties of the dynamically induced dipolar distribution. We find that under resonant conditions, scaling with the geometric fractal dimension is only observed for systems much larger than a length scale that is related to the linewidth of each individual resonance. The relevance to this result for the interpretation of light scattering experiments is discussed.

DOI: 10.1103/PhysRevB.67.184204 PACS number(s): 61.43.Hv, 89.75.Da, 42.25.Dd, 78.66.Sq

I. INTRODUCTION

Many objects in nature[1] have a geometry that is best described as fractal. Such is the case of colloidal aggregates which are scale invariant within a range of length scales bounded from below by the size of each individual monomer and from above by the size of the complete system. The number of colloidal particles $N(R)$ within a ball of radius R increases as a power law R^{d_f}. The exponent d_f, known as the fractal dimension, is lower than the topological dimension d of the space in which the object is embedded and is frequently a noninteger. Similarly, the correlation function $C(\vec{r})$, proportional to the probability of finding two particles a separation $\vec{r}$ apart, scales as r^{d_f-d}. In order for the fractal geometry to manifest itself, the highest and lowest length scales should be far apart, and thus the aggregate must contain a very large number of particles. For this reason, the simulation of physical properties of an aggregate, such as their optical properties, usually requires a large scale computation.

Early works proposed simple models for the computational simulation of several fractal structures found in nature. Such is the case of diffusion-limited aggregation,[2] diffusion-limited cluster aggregation (DLCA),[3] reaction-limited aggregation,[4] and reaction-limited cluster aggregation.[5] The increase of computational capacity and the development of algorithms has allowed the solution of problems involving many interacting bodies.[6] Since the 1980s, algorithms employing multiple length and time scales have been employed to treat many-particle interacting systems.[7] They have been most useful for simulations in astrophysics and cosmology which involve a large number of particles subject to the unscreened long-range gravitational interaction.[8] Frequently, this kind of method employs a binary tree data organization scheme where the lengthscales are refined as the tree is climbed. Fast multipole methods[9] combine multipole expansions with the multiresolution approach and have proved advantageous for attacking manifold classical problems with a large number of interacting parts. In the case of fractal aggregates, the multiresolution approach has been applied to simulate the growth of clusters with up to 10^6 particles.[10]

In this work we develop a hierarchical multilengthscale algorithm that employs a binary tree data structure and allows the simulation of the growth of large aggregate clusters as well as an efficient calculation of their optical properties taking full account of the long range of the electromagnetic interactions between monomers. We employ this algorithm to explore the problem of scattering from fractal structures in the resonant regime and to shed light on the problem of the interpretation of the scattering data.

Throughout the last two decades, the scattering of light has been an important experimental tool in the study of the physics of fractal systems.[11–15] Light scattering has frequently been interpreted within the first Born approximation, which accounts only for single scattering events. This means that each particle in the aggregate is assumed to respond to the incoming field only, but does not ''feel'' the field produced by the rest of the particles. In this case, the angular distribution of the light statically scattered, characterized by the differential cross section $d\sigma/d\Omega$, is proportional to the structure factor $S(\vec{Q})$, which, being simply the Fourier transform of $C(\vec{r})$ with scattering wave vector $\vec{Q}$, scales for a fractal of dimension d_f as Q^{-d_f}. For small scattering angles θ, $\vec{Q}$ is orthogonal to the wave vector of the incident light and $Q \approx (\omega/c)\theta$, where ω is the frequency. Thus, information about the geometry of the system may be obtained by measuring $d\sigma/d\Omega$. In particular, from the decay of the intensity with angle we may infer the fractal dimension.[16]

The general validity of the first Born approximation is questionable,[17] especially for frequencies close to a resonance. For those frequencies, the response of each particle is expected to be very large. Therefore, its interactions with nearby particles should not be neglected. A significant effort has been done to understand the optical properties of fractal aggregates, for which optically active resonant modes with a

very high local field concentrated in just a few small regions have been reported.[18] The number of these *hot spots*, their position, and their mutual distances have been shown[19,20] to vary abruptly with frequency, so that the spatial distribution of the intensity cannot be characterized by a single localization length. Although the normal modes display inhomogeneous localization and are neither localized nor extended in the usual sense, in a recent work[21] we obtained that even when multiple scattering is accounted for, it is still possible to get an approximate power law decay for the scattered intensity as in the case of single scattering, but only at some spectral regions, while no scaling at all was found at other regions. In this work we do a more thorough research into this scaling, we analyze the local field intensity distribution at different resonant regions, and we find the conditions under which scaling is to be expected.

For definitiveness, in this paper we chose a particular class of systems, namely, those formed by the process of diffusion limited cluster-cluster aggregation[3] of spherical particles. To simplify the visualization and the interpretation of the results, we limit ourselves to aggregates lying on a flat surface illuminated by light impinging in the direction normal to the surface. We further assume that the wavelength λ is much larger than the radius R_0 of a single sphere and that the interactions among the spheres are dominated by the nonretarded part of the dipole-dipole interaction.

The structure of the paper is the following. Section II contains our theory: First we set up a perturbative calculation of the local field and the induced dipoles (Sec. II A) with which we present the hierarchical data structures and algorithms that allow efficient calculations for problems with a large number of particles (Sec. II B), and which we later generalize to the non-perturbative regime (Sec. II C). The resulting dipole moments are employed to calculate the scattering of light (Sec. II D), the susceptibility of the system, and its normal electromagnetic modes (Sec. II E). In order to visualize, discuss, and interpret our results, in Sec. III we present a simplified scalar model of dipolarly interacting particles which we employ to present results for DLCA aggregates grown in 2D: We obtain the normal mode spectrum for systems composed of arbitrary materials and study the details of individual resonances at various spectral regions, their hot spot structure, and their localization properties (Sec. III A). We also study the scattering (Sec. III B), its dependence on wave vector and its scaling behavior. We find that scaling with the geometrical fractal dimension is approximately obeyed but only within certain regions of the spectrum. Further inquiry reveals, though, that scaling can be observed at any spectral region provided the system is larger than certain lengthscale which depends on the linewidth of the resonances of the system, and therefore, on the dissipative part of its dielectric response. Since the scalar model employed in Sec. III is equivalent to the excitation of longitudinal dipoles with a longitudinal field, it is unsuitable for a quantitative calculation of electromagnetic scattering. Thus, in Sec. IV we present the corresponding results for a full vectorial calculation. We find that the qualitative aspects of our most important results carry over into the transverse regime. Thus, they have to be taken into account for the correct interpretation of light scattering experiments. Finally, Sec. V is devoted to conclusions.

II. THEORY

A. Local field

We consider an aggregate made up of $N \gg 1$ small spherical particles of radius R_0 with dielectric function ϵ embedded within a host with response function ϵ_h. When a long-wavelength field $\vec{E}$ acts on one sphere, it induces a dipole moment $\vec{p} = \gamma \vec{E}$, where the monomer polarizability γ is given by

$$\gamma = \frac{\epsilon - \epsilon_h}{\epsilon + 2\epsilon_h} R_0^3. \tag{1}$$

Thus, when an incoming optical field $\vec{E}_i^{\,\mathrm{ex}} \equiv \vec{E}^{\,\mathrm{ex}}(\vec{r}_i)$ shines on the system, each particle acquires a dipole

$$\vec{p}_i = \gamma \left(\vec{E}_i^{\,\mathrm{ex}} + \sum_j \vec{\mathbb{t}}_{ij} \cdot \vec{p}_j \right) \tag{2}$$

$(i = 1 \ldots N)$, where $\vec{\mathbb{t}}_{ij} \equiv \vec{\mathbb{t}}(\vec{r}_i - \vec{r}_j)$ is the dipolar interaction between the ith and jth spheres located at positions $\vec{r}_i$ and $\vec{r}_j$, respectively. The distance between near neighbor particles in an aggregate is of the order of their size, as close neighbors within an aggregate might touch each other. Therefore, the local field variation across each monomer would lead to a coupling of the dipole moment to higher order multipoles. The optical spectra of the system would have features arising from this coupling, such as peaks arising from the multipolar resonances of each individual particle.[22] Quantitative calculations for specific aggregates might have to take this into account. For example, it has been argued that multipolar interactions are responsible for the infrared wing observed in the absorption spectra of some silver colloidal aggregates.[23] Multipolar effects may be accounted by replacing $\vec{p}_i$ and $\vec{p}_j$ in Eq. (2) by the *vectors* of multipolar moments q_i^{lm} and $q_j^{l'm'}$, the polarizability γ by the multipolar polarizabilities γ^l, the field $\vec{E}_i$ by the spherical irreducible components of its spatial derivatives $\nabla^{(l-1)}\vec{E}_i$ of order $l-1$, and the tensor $\vec{\mathbb{t}}_{ij}$ by the interaction matrix $t_{ij}^{lml'm'}$ which couples the m'th component of a multipole of order l' at $\vec{r}_j$ to the mth component of a multipole of order l at $\vec{r}_i$.[24,25] Nevertheless, we believe that multipolar interactions are nonessential for the understanding of the *scaling* properties of the scattered light which constitute the subject matter of this paper, and the additional structures they introduce into the spectra actually obscure their analysis. It has been shown that solving Maxwell equations numerically in disordered systems leads to qualitatively similar results as employing the dipolar approximation.[26] As it is, Eq. (2) would be exact for a *model system* made up of point polarizable particles, instead of spheres, with given polarizability γ and located at the centers of the particles that make up the actual aggregate. As multipolar effects are known to decay extremely fast as the interparticle distance increases,[24,25] Eq.

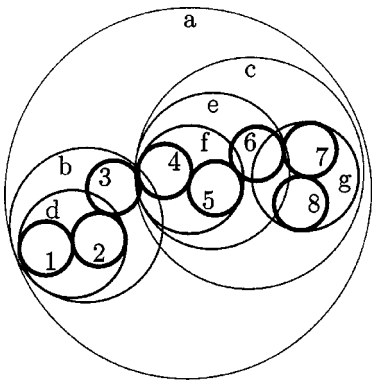

FIG. 1. Small aggregate made up of particles 1,2, . . . 8 organized hierarchically into groups $a,b,\ldots g$.

(2) is also appropriate for aggregates whose particles are coated with an optically inactive separator.[27] We remark that it is a common practice to coat colloidal particles in order to control their agregation kinematics.[28] For these reasons, we have neglected multipoles in Eq. (2).

B. Hierarchical representation

In the limiting case of a very small polarizability $\gamma \ll R_0^3$, the induced field is much smaller than the external field and Eq. (2) may be solved by an iterative process. In this case we write

$$\vec{p}_i^{\,0} = \gamma \vec{E}_i^{\,\mathrm{ex}}, \tag{3}$$

$$\vec{p}_i^{\,n+1} = \gamma(\vec{E}_i^{\,\mathrm{ex}} + \vec{E}_i^{\,n+1}) = \gamma\left(\vec{E}_i^{\,\mathrm{ex}} + \sum_j \overleftrightarrow{t}_{ij} \cdot \vec{p}_j^{\,n}\right), \tag{4}$$

and iterate over the scattering order $n=0,1,\ldots$ until we converge to the fixed point $\vec{p}_i = \vec{p}_i^{\,\infty}$ which is the desired solution. Although this method[29] has obvious limitations, it has found some useful applications.[30] We use this order-of-scattering method to present our hierarchical algorithm and our tree data structure. In Sec. II C we will generalize our calculation methods to the more interesting resonant situations for which iteration (4) is not adequate.

The most time consuming step when applying the method above is the repeated evaluation of the induced field $\vec{E}_i^{\,n+1}$ at all positions $\vec{r}_i$ due to all the other dipoles $\vec{p}_j^{\,n}$ at $\vec{r}_j$, which naively would require $O(N^2)$ steps. To accelerate the calculation we introduce the concept of *hierarchical groups* of particles as follows. The whole aggregate constitutes a single group at the highest level of the hierarchy. It is composed of exactly two groups at the next hierarchical level, each containing a connected fragment of the original aggregate. Each of these subgroups is itself divided into two smaller groups containing connected fragments of the corresponding subcluster. We proceed with this division obtaining smaller and smaller subclusters until we reach *atomic groups* made up of only one particle. Figure 1 illustrates this hierarchical structure for a particular small aggregate. In it, particles 1 and 2 form a group *d*, which together with particle 3 constitutes group *b*. Adding group *c*, which is built similarly from particles 4 . . . 8, we finally obtain the whole aggregate *a*. The hierarchical group structure may be described by a binary tree (Fig. 2) whose root represents the whole system, whose internal nodes represent subgroups which decrease in size as we climb the tree, and whose leaves represent the individual particles.

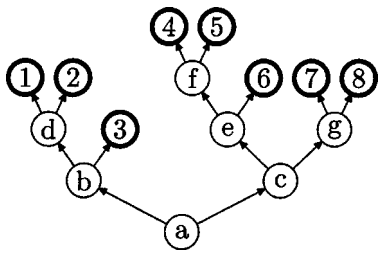

FIG. 2. A binary tree representation of an eight-particle aggregate according to the group structure displayed in Fig. 1.

Each *group* α, either atomic or composite, is characterized by its number of particles N_α and by a sphere of radius R_α centered on $\vec{r}_\alpha$. We chose $\vec{r}_\alpha$ at the center of mass of the particles composing the group and we chose R_α large enough to circumscribe all of the particles belonging to the group. Although the spheres corresponding to different groups may overlap one another, and a given particle may be covered by more than one sphere, group membership is chosen in such a way that there are no cycles in the tree representing the aggregate. There are many different group hierarchies that may represent the same aggregate. We employ a strategy that arranges particles according to their relative distance in order to minimize the overlap between the spheres representing different groups and that attempts to balance both the radius and the number of particles of the subgroups that emerge from any given node. The details of this strategy will be presented elsewhere.[31] The number of nodes of the tree, including its root and its leaves is $2N-1$, independently of the tree structure. The height of the tree does depend on the structure, and is given by $\log_2 N$ in the optimum case of a perfectly balanced tree.

To each group we additionally assign physical properties like those of its constitutive particles, according to the specific physical problem we want to solve.[31] In the present case, we assign to each group ζ its total dipole moment

$$\vec{p}_\zeta \equiv \sum_{i \in \zeta} \vec{p}_i, \tag{5}$$

where the sum is taken over all the particles *i* belonging to the group ζ, which we abbreviate as $i \in \zeta$. Since each nonatomic group ζ contains exactly two subgroups, which we designate as its *daughter* ζ^d and its *son* ζ^s, its total dipole may be updated recursively as

$$\vec{p}_\zeta = \vec{p}_{\zeta^d} + \vec{p}_{\zeta^s}. \tag{6}$$

Going back to the evaluation of $\vec{p}_i^{\,n+1}$, we notice that each contribution of the form $\Sigma_{j \in \zeta} \overleftrightarrow{t}_{ij} \cdot \vec{p}_j^{\,n}$ in Eq. (4) may be replaced by a single term $\overleftrightarrow{t}_{i\zeta} \cdot \vec{p}_\zeta^{\,n}$ *if* R_ζ is small enough and $r_{i\zeta}$

large enough that we may approximate $\overleftrightarrow{t}_{ij} \approx \overleftrightarrow{t}_{i\zeta} \equiv \overleftrightarrow{t}(\vec{r}_i - \vec{r}_\zeta)$. In this case, we replace the individual interactions $\overleftrightarrow{t}_{ij}$ between the ith particle and the N_ζ individual particles $j \in \zeta$ that make up group ζ by the single interaction $\overleftrightarrow{t}_{i\zeta}$ between particle i and a fictitious particle ζ located at $\vec{r}_\zeta$ and carrying the algebraic sum $\vec{p}^{\,n}_\zeta$ of the dipole moments $\vec{p}^{\,n}_j$ of all the particles $j \in \zeta$. For example, in Fig. 1 we might replace the two interactions between particle numbered 1 and particles 7 and 8 by a single interaction between particle 1 and group g. If we are willing to tolerate larger computational errors, we could even replace the five interactions between particle 1 and particles 4 . . . 8 by a single interaction between particle 1 and group c.

It is simple to implement the ideas above in a recursive fashion. Calling $\vec{E}_{i\alpha}$ the field induced at $\vec{r}_i$ by all particles $j \in \alpha$, we calculate

$$\vec{E}_{i\alpha} = \begin{cases} \overleftrightarrow{t}_{i\alpha} \vec{p}_\alpha & \text{if } R_\alpha \text{ is } \textit{small} \\ \vec{E}_{i\alpha^d} + \vec{E}_{i\alpha^s} & \text{otherwise,} \end{cases} \tag{7}$$

where by *small* we mean that $R_\alpha / r_{i\alpha} < \Lambda$ or that the group contains only a single particle. Here, Λ is a dimensionless parameter between 0 and 1 which controls the speed and accuracy of the computation.[31] $\Lambda = 0$ leads to the exact result but with no speed gain, while with $\Lambda = 1$ the calculation is done in just one step, but the result would be completely inaccurate and therefore meaningless. The first correction to the approximation $\vec{E}_{i\zeta} \approx \overleftrightarrow{t}_{i\zeta} \cdot \vec{p}_\zeta$ is given by $\nabla_i \overleftrightarrow{t}_{i\zeta} : \overleftrightarrow{Q}_\zeta$, where $\overleftrightarrow{Q}_\zeta$ is the quadrupole moment of the composite group ζ. As $\nabla_i \overleftrightarrow{t}_{i\zeta} \sim O(t_{i\zeta}/r_{i\zeta})$ and $\overleftrightarrow{Q}_\zeta \sim O(p_\zeta R_\zeta)$, we expect that the approximation leads to a relative error of order $O(R_\zeta / r_{i\zeta})$. Thus, Λ is a measure of the relative error we are prepared to allow in the calculation of the field produced by any one group. The error is actually much smaller as the *centers of electric polarization* of a group, i.e., the average position of its particles weighted by the components of the dipolar moments, are frequently close to the center of mass, yielding a relatively small quadrupole moment for the group $Q_\zeta \ll p_\zeta R_\zeta$. To take retardation effects into account, we have to consider the wavelength λ as another length scale for the spatial variation of the induced field and we have to complement the conditions above with $R_\alpha / \lambda < \Lambda$. Finally, Eq. (4) can be recast as

$$\vec{p}^{\,n+1}_i = \gamma(\vec{E}^{\,\mathrm{ex}}_i + \vec{E}^{\,n}_{ia}), \tag{8}$$

where a denotes the root of the tree that represents the whole aggregate and $\vec{E}^{\,n}_{ia}$ is calculated recursively employing Eq. (7). The algorithm above may be modified simply adding higher multipoles to the groups. The corresponding advantages of permitting a more accurate calculation of the induced field for a given Λ have to be weighted against the computational cost of storing and updating the multipolar moments of each group in the hierarchy.

C. Noniterative solution

The iterative solution of Eq. (2) to obtain the dipole moments is not feasible if the polarizability γ is not small, or more generally, as γ approaches a resonance of the system, since the sequence of successive scattering orders might diverge. Even in this case, the hierarchical representation of the aggregate is useful. First, we rewrite Eq. (2) as the matrix equation

$$\mathbf{M}\mathbf{p} \equiv [(1/\gamma)\mathbf{1} - \mathbf{T}]\mathbf{p} = \mathbf{E}^{\mathrm{ex}}, \tag{9}$$

where the dipole moments of all the particles and the external field are represented by the block column vectors $\mathbf{p} = (\vec{p}_1, \vec{p}_2, \ldots \vec{p}_N)^T$ and $\mathbf{E}^{\mathrm{ex}} = (\vec{E}^{\,\mathrm{ex}}_1, \vec{E}^{\,\mathrm{ex}}_2, \ldots \vec{E}^{\,\mathrm{ex}}_N)^T$ respectively, $\mathbf{1}$ denotes the unit matrix,

$$\mathbf{T} = \begin{pmatrix} \overleftrightarrow{t}_{11} & \overleftrightarrow{t}_{12} & \ldots & \overleftrightarrow{t}_{1N} \\ \overleftrightarrow{t}_{21} & \overleftrightarrow{t}_{22} & \ldots & \overleftrightarrow{t}_{2N} \\ \vdots & \vdots & \ddots & \vdots \\ \overleftrightarrow{t}_{N1} & \overleftrightarrow{t}_{N2} & \ldots & \overleftrightarrow{t}_{NN} \end{pmatrix} \tag{10}$$

represents the dipolar interactions, and $(\cdots)^T$ denotes the transpose of the matrix $(\cdots)$. Notice that in general Eq. (9) is a $3N \times 3N$ matrix equation, and that, due to the long range of the dipole-dipole interaction, the matrices $\mathbf{M}$ and $\mathbf{T}$ are *dense*. This is at the core of the numerical difficulty of solving Eq. (9) for large systems. Now we build a new vector $\mathbf{p}'$ by appending the dipole moments of the $N-1$ groups to those of the N particles, i.e., $\mathbf{p}' \equiv (\vec{p}_1, \vec{p}_2 \ldots \vec{p}_N, \vec{p}_{\lambda_1}, \vec{p}_{\lambda_2} \ldots \vec{p}_{\lambda_{N-1}})^T$, where λ_i runs over the $N-1$ composite group indices ζ. By appending the $3(N-1)$ conditions [Eqs. (6)] to the $3N$ equations [Eqs. (2)] we end up with a $3(2N-1) \times 3(2N-1)$ system

$$\mathbf{M}'\mathbf{p}' \equiv \left[\begin{pmatrix} \mathbf{M} & \mathbf{0} \\ \mathbf{0} & \mathbf{1} \end{pmatrix} - \begin{pmatrix} \mathbf{0} \\ \mathbf{C} \end{pmatrix} \right] \mathbf{p}' = \begin{pmatrix} \mathbf{E}^{\mathrm{ex}} \\ \mathbf{0} \end{pmatrix} \equiv (\mathbf{E}^{\mathrm{ex}})', \tag{11}$$

where $\mathbf{M}$ is the same $3N \times 3N$ matrix as in Eq. (9), $\mathbf{0}$ represents appropriately sized matrices filled with zeroes and $\mathbf{C}$ is the $3(N-1) \times 3(2N-1)$ group connectivity matrix that describes the tree structure and has elements

$$C_{\zeta\alpha} = (\delta_{\zeta^d \alpha} + \delta_{\zeta^s \alpha}) \overleftrightarrow{1} = \begin{cases} \overleftrightarrow{1} & \text{if group } \zeta \text{ is the } \textit{father of group } \alpha \\ \overleftrightarrow{0} & \text{otherwise,} \end{cases} \tag{12}$$

where $\delta_{\zeta^d \alpha}$ and $\delta_{\zeta^s \alpha}$ are Kronecker deltas and $\overleftrightarrow{1}$ denotes the unit 3×3 tensor.

Rewriting the system of equations (9) as Eq. (11) increases the number of equations and unknowns from $3N$ to $3(2N-1)$. However, we may take advantage of the hierarchical representation of the aggregate in order to manipulate matrix $\mathbf{M}'$ and reduce considerably the computational cost of solving Eq. (11). Thus, whenever R_ζ is small enough as compared to $r_{i\zeta}$, in the same sense as in Eq. (7), we may replace the N_ζ entries $\overleftrightarrow{t}_{ij}, (j \in \zeta)$ with block indices ij by the null tensor $\overleftrightarrow{0}$ if we simultaneously perform the single replacement

$\overleftrightarrow{0} \rightarrow \overleftrightarrow{t}_{i\zeta}$ at the block with indices $i\zeta$. With this procedure we can reduce significantly the number of non-zero elements of $\mathbf{M}'$ producing a *sparse matrix* $\mathbf{M}''$ such that solving the equation

$$\mathbf{M}''\mathbf{p}'' = \begin{pmatrix} \mathbf{E}^{\mathrm{ex}} \\ \mathbf{0} \end{pmatrix} \tag{13}$$

for aggregates with a very large number N of particles becomes computationally feasible using a variety of methods,[32,33] while the solution $\mathbf{p}''$ approximates the desired solution $\mathbf{p}'$ with an arbitrary accuracy, controlled by the parameter Λ.

As an example, consider the aggregate shown in Figs. 1 and 2. The corresponding matrix $\mathbf{M}'$ is given by

$$\mathbf{M}' = \begin{array}{c} \begin{array}{cccccccccc} 1 & 2 & 3 & 4 & \ldots & 8 & a & b & c & d & \ldots \end{array} \\ \begin{pmatrix} \overleftrightarrow{M}_{11} & -\overleftrightarrow{t}_{12} & -\overleftrightarrow{t}_{13} & -\overleftrightarrow{t}_{14} & \ldots & -\overleftrightarrow{t}_{18} & \overleftrightarrow{0} & \overleftrightarrow{0} & \overleftrightarrow{0} & \overleftrightarrow{0} & \ldots \\ \vdots & & & & \ddots & & & & & & \ddots \\ \overleftrightarrow{0} & \overleftrightarrow{0} & \overleftrightarrow{0} & \overleftrightarrow{0} & \ldots & \overleftrightarrow{0} & \overleftrightarrow{1} & -\overleftrightarrow{1} & -\overleftrightarrow{1} & \overleftrightarrow{0} & \ldots \\ \overleftrightarrow{0} & \overleftrightarrow{0} & -\overleftrightarrow{1} & \overleftrightarrow{0} & \ldots & \overleftrightarrow{0} & \overleftrightarrow{0} & \overleftrightarrow{1} & \overleftrightarrow{0} & -\overleftrightarrow{1} & \\ \vdots & & & & \ddots & & & & & & \ddots \end{pmatrix} \end{array} \begin{array}{c} \leftarrow \\ \\ \leftarrow \\ \leftarrow \\ \\ \end{array} \begin{array}{c} 1 \\ \vdots \\ a \\ b \\ \vdots \end{array} . \tag{14}$$

The first row of this matrix indicates the interactions of the first particle with the external field and with particles 2 . . . 8. Rows 2 . . . 8 are similar. On the other hand, row *a* states that the dipole moment of the whole aggregate *a* is simply the sum of the dipole of group *b* plus that of group *c*. Similarly, row *b* indicates that group *b* is made up of particle 3 and group *d*. The remaining rows are analogous.

Assuming that group *c* of Fig. 1 may be considered *small enough and far enough* from particle 1, so that the five interactions t_{1j} $(j \in c \leftrightarrow \{4 \ldots 8\})$ may be replaced by a single interaction t_{1c}, the resulting matrix $\mathbf{M}''$ would look like

$$\mathbf{M}'' = \begin{array}{c} \begin{array}{cccccccccc} 1 & 2 & 3 & 4 & \ldots & 8 & a & b & c & d & \ldots \end{array} \\ \begin{pmatrix} \overleftrightarrow{M}_{11} & -\overleftrightarrow{t}_{12} & -\overleftrightarrow{t}_{13} & \overleftrightarrow{0} & \ldots & \overleftrightarrow{0} & \overleftrightarrow{0} & \overleftrightarrow{0} & -\overleftrightarrow{t}_{1c} & \overleftrightarrow{0} & \ldots \\ \vdots & & & & \ddots & & & & & & \ddots \end{pmatrix} \end{array} \begin{array}{c} \leftarrow \\ \\ \end{array} \begin{array}{c} 1 \\ \vdots \end{array} . \tag{15}$$

Comparing Eqs. (15) and (14) we can appreciate the increase in the number of null elements. It is unlikely that group *c* could actually be considered far enough from particle 1 in the particular aggregate shown in Fig. 1 to permit this particular replacement. However, similar replacements may safely be done for larger systems without introducing appreciable errors, the resulting savings become considerable[31] for realistic cases and they increase with the size of the aggregates. As matrix $\mathbf{M}''$ may be simply constructed on the fly from the distances $\vec{r}_{i\alpha}$ and the tree structure of the aggregate, it is not even necessary to store its relatively few non-null elements.

A hierarchical approach to the calculation of the electromagnetic response of fractal systems has been previously employed by Claro and Fuchs.[34] In that calculation, each group in the hierarchy was replaced by a single *particle* with an appropriate size and with a renormalized response calculated iteratively in terms of the *particles* it contains one level below in the hierarchy; each group was considered indivisible after that replacement and when calculating its interaction with neighbor groups. This constitutes an essential difference from our present scheme, in which each particle responds *individually* to the local field that polarizes it. When calculating that field we treat whole groups of particles as a single dipole, but *only* if that group happens to be small enough and far away enough so that this replacement does not introduce an appreciable error. Otherwise, we *open* the group and consider recursively the field produced by its subgroups or by its particles. Thus, with our procedure we can obtain the local field with an arbitrary accuracy. The renormalization procedure of Claro and Fuchs would lead to errors and would not be applicable unless there is a large enough distance between all groups at each level in the hierarchy, as compared to their size. For the colloidal aggregates we consider here, neighboring groups might overlap each other (see Fig. 1), so that the approach of Ref. 34 is not applicable.

D. Scattering

Once we have obtained $\vec{p}_j$, we can proceed to the calculation of the differential scattering cross section $d\sigma/d\Omega$. We assume that the the external field is a long-wavelength incoming wave

$$\vec{E}_j^{\rm ex}=\vec{E}_0 e^{i(\vec{q}_{\rm in}\cdot\vec{r}_j-\omega t)} \tag{16}$$

of frequency ω and wave vector $\vec{q}_{\rm in}=q_0\hat{q}_{\rm in}$ and with $q_0R_0 \ll 1$, where the hat denotes a unit vector. The scattered field is simply the sum of the far fields radiated by all of the dipoles $\vec{p}_j$. Factoring out from the induced dipoles the phase and magnitude of the incident field and normalizing away its units employing the distance R_0 through the definition

$$\vec{p}_j=\vec{d}_j R_0^3 E_0 e^{i(\vec{q}_{\rm in}\cdot\vec{r}_j-\omega t)}, \tag{17}$$

we calculate Poynting's vector and we obtain the differential scattering cross section per unit solid angle in the direction $\hat{q}_{\rm out}$,

$$d\sigma/d\Omega=\epsilon_h(q_0R_0)^4 N R_0^2\langle|\vec{D}^{\perp}(\vec{Q})|^2\rangle, \tag{18}$$

where $\vec{Q}=\vec{q}_{\rm out}-\vec{q}_{\rm in}$ is the scattering wave vector, $\vec{q}_{\rm out}=q_0\hat{q}_{\rm out}$ is the outgoing wave vector in the observation direction, $\vec{D}(\vec{Q})$ is a Fourier representation of the normalized induced dipoles

$$\vec{D}(\vec{Q})\equiv\frac{1}{\sqrt{N}}\vec{d}(\vec{Q})\equiv\frac{1}{\sqrt{N}}\sum_j \vec{d}_j e^{-i\vec{Q}\cdot\vec{r}_j}, \tag{19}$$

and the superscript $\perp$ denotes the transverse projection $\vec{D}^{\perp}(\vec{Q})$ of $\vec{D}(\vec{Q})$, perpendicular to $\hat{q}_{\rm out}$. For disordered systems we add an ensemble average, denoted by the angular brackets.

We take advantage again of the hierarchical data structure to accelerate the calculation of the scattering cross section by replacing the contribution $d_\zeta(\vec{Q})\equiv\Sigma_{j\in\zeta}\vec{d}_j e^{-i\vec{Q}\cdot\vec{r}_j}$ to the sum in Eq. (19) by the single term $\vec{d}_\zeta(0)e^{-i\vec{Q}\cdot\vec{r}_\zeta}$ whenever the size R_ζ of the group ζ and the wave vector $\vec{Q}$ are small enough, $QR_\zeta\ll 1$, so that we can approximate $e^{-i\vec{Q}\cdot\vec{r}_j}\approx e^{-i\vec{Q}\cdot\vec{r}_\zeta}$ for all particles $j\in\zeta$. Thus, we write

$$\vec{D}(\vec{Q})=\frac{1}{\sqrt{N}}\vec{d}_a(\vec{Q}), \tag{20}$$

and evaluate recursively

$$\vec{d}_\alpha(\vec{Q})=\begin{cases}\vec{d}_\alpha(0)e^{-i\vec{Q}\cdot\vec{r}_\alpha} & \text{if } R_\alpha \text{ is } \textit{small}\\ \vec{d}_{\alpha^d}(\vec{Q})+\vec{d}_{\alpha^s}(\vec{Q}) & \text{otherwise.}\end{cases} \tag{21}$$

E. Normal modes

Before studying the scattering of light by fractal aggregates at resonance, it is convenient to characterize their normal electromagnetic modes. The normal modes depend on the geometry of the system as well as on its composition. However, the later dependence may be factored out employing Bergman's spectral density theory.[35] To this end, we define a spectral variable

$$u\equiv\frac{1}{(1-\epsilon/\epsilon_h)}, \tag{22}$$

so that

$$1/\gamma=(1-3u)/R_0^3. \tag{23}$$

Using Dirac's notation we represent the incoming field by a ket $|E^{\rm ex}\rangle\equiv\mathbf{E}^{\rm ex}\equiv\sqrt{N}E_0|0\rangle$, where $|0\rangle$ is normalized, $\langle 0|0\rangle=1$. The induced dipole moment can similarly be represented by a ket $|p\rangle\equiv\mathbf{p}$. The work done per unit time by the external field due to the presence of the spheres, $\mathcal{P}=\omega\,{\rm Im}(\Sigma_j(\vec{E}_j^{\rm ex})^*\cdot\vec{p}_j)/2$, may therefore be written as

$$\mathcal{P}=\omega V\,{\rm Im}(\chi)|E_0|^2/2, \tag{24}$$

where $V=4\pi NR_0^3/3$ is the total volume occupied by the N spheres of radius R_0 that make up the aggregate, and

$$\chi=\frac{3}{4\pi}\langle 0|[(1-3u)\mathbf{1}-R_0^3\mathbf{T}]^{-1}|0\rangle \tag{25}$$

is a macroscopic dimensionless susceptibility. The normal modes of the system are the oscillations it can sustain in the absence of an external field, and can therefore be identified with the poles of the susceptibility $\chi(u)$.

For dissipationless spheres made up of a Drude conductor within vacuum, we can identify $u=\omega^2/\omega_p^2$, where $\epsilon(\omega)=1-\omega_p^2/\omega^2$ and ω_p is the plasma frequency of the conductor. Thus, u is frequently identified with ω. For example, a resonance with a relatively large or small u may be called *blue* or *red* respectively. We will follow this practice, although the actual frequency corresponding to a given u depends on the material properties of both the spheres and the host implicitly through $\epsilon(\omega)$ and $\epsilon_h(\omega)$. Thus it is in general a complex valued, complicated nonmonotonic function.

By writing $\mathbf{T}$ in terms of its normalized eigenvectors $|t_n\rangle$, with a corresponding eigenvalue t_n, we may rewrite

$$\chi=\frac{3}{4\pi}\sum_n\frac{\langle 0|t_n\rangle\langle t_n|0\rangle}{1-3u-R_0^3t_n}. \tag{26}$$

Notice that in the absence of retardation, the dipolar interaction

$$\vec{\vec{t}}_{ij}=\frac{3\vec{r}_{ij}\vec{r}_{ij}-r_{ij}^2\vec{\vec{1}}}{r_{ij}^5}(1-\delta_{ij}) \tag{27}$$

is independent of ϵ and of ϵ_h, and therefore χ depends on the materials forming the system only through the variable u in the denominator. Thus, Eq. (26) is a particular case of the Bergman representation[35] for the response of an arbitrary composite made up of two materials with different dielectric properties. Bergman's theory may be set up for an arbitrary composite by noticing that[36] within a transparent dissipationless host ($\epsilon_h>0$), the whole aggregate will be an energy sink ($\chi''>0$) or an energy source ($\chi''<0$) whenever the inclusions themselves consume electromagnetic energy ($\epsilon''>0$, as expected in thermodynamic equilibrium) or produce it ($\epsilon''<0$, as in a pumped system out of equilibrium such as

a linear optical amplifier) respectively. Here, we abbreviate $(\cdots)'' \equiv \mathrm{Im}(\cdots)$. Thus, χ'' has the same sign as u'', and consequently its poles are necessarily simple and located at the real, $u''=0$, axis. From Eq. (24), these poles correspond to the optically active normal modes of the system. As it is thermodynamically allowed to have materials in equilibrium with any static value $\epsilon>1, \epsilon_h>1$, no poles of χ may appear for $\epsilon/\epsilon_h>0$. Thus, all the normal modes of the system are confined to the interval $0 \leqslant u \leqslant 1$. Finally, using Cauchy's integral formula we obtain

$$\chi(u)=\frac{1}{4\pi}\sum_n \frac{C_n}{s_n-u}, \tag{28}$$

where the sum is taken over all the poles $s_n \in [0,1]$ of χ, $C_n=-4\pi\mathcal{R}_n>0$, and $\mathcal{R}_n$ are the corresponding residues of χ. An equivalent expression is

$$\chi(u)=\frac{1}{4\pi}\int_0^1 ds \frac{g(s)}{s-u}, \tag{29}$$

where $g(s)=\Sigma_n C_n \delta(s-s_n)$ is the normalized spectral density function. Equation (29) may be inverted, yielding

$$g(s)=4\ \mathrm{Im}\,\chi(s^+), \tag{30}$$

where $s^+ \equiv \lim_{\Gamma\to 0^+} s+i\Gamma$. Comparing Eqs. (28) and (29) with Eq. (26) lets us identify

$$C_n=|\langle 0|t_n\rangle|^2 \tag{31}$$

and

$$s_n=(1-R_0^3 t_n)/3, \tag{32}$$

and interpret

$$g(s)=\sum_n |\langle 0|t_n\rangle|^2 \delta(s-s_n) \tag{33}$$

as a density of states projected unto the *initial* state $|0\rangle$ defined by the external field.

Alternative spectral representations of the response of fractal aggregates[18–20] have appeared in the literature, but they can be trivially mapped to the one above. There are well known sum rules for the Bergman's spectral function. In the present context, we obtain one of them by integrating Eq. (33) with respect to s, obtaining

$$\int_0^1 ds\, g(s)=\sum_n \langle 0|t_n\rangle\langle t_n|0\rangle=\langle 0|0\rangle=1, \tag{34}$$

where we used the completeness of the basis $\{|t_n\rangle\}$. A second sumrule may be obtained by taking the first moment of $g(s)$,

$$\int_0^1 ds\, sg(s)=\sum_n \langle 0|t_n\rangle(1-R_0^3 t_n)\langle t_n|0\rangle/3$$
$$=(1-R_0^3\langle 0|\mathbf{T}|0\rangle)/3, \tag{35}$$

and then averaging over the direction of the external field,

$$\int_0^1 ds\, s\overline{g}(s)=1/3, \tag{36}$$

where we denote the angular average of any quantity $(\cdots)$ by $\overline{(\cdots)}$ and we used the fact that $\overline{t_{ij}}=0$, as may be verified directly from Eq. (27).

By defining a *Hamiltonian*

$$\mathbf{H}\equiv(\mathbf{1}-R_0^3\mathbf{T})/3, \tag{37}$$

and its corresponding Green's operator

$$\mathbf{G}(u)\equiv(u\mathbf{1}-\mathbf{H})^{-1}, \tag{38}$$

we may identify[37]

$$\chi(u)=-\frac{1}{4\pi}G_{00}(u). \tag{39}$$

Thus, we may use well known methods developed for the calculation of the projected Green's function of electronic systems and adapt them[23,38] to the calculation of the susceptibility.[39] An efficient evaluation of $\chi(u)$ and $g(s)$ may be carried out employing the Haydock recursion method.[40–42] By acting repeatedly on the ket $|0\rangle$ with $\mathbf{H}$ and othonormalizing the resulting vectors, we construct a basis $\{|k\rangle\}$ in which $\mathbf{H}$ becomes tridiagonal,

$$\mathbf{H}=\begin{pmatrix} a_0 & b_1 & 0 & 0 & \cdots \\ b_1 & a_1 & b_2 & 0 & \\ 0 & b_2 & a_2 & b_3 & \\ \vdots & & & \ddots & \end{pmatrix}, \tag{40}$$

where

$$b_{k+1}|k+1\rangle \equiv \mathbf{H}|k\rangle - a_k|k\rangle - b_k|k-1\rangle, \tag{41}$$

$$a_k=\langle k|\mathbf{H}|k\rangle, \tag{42}$$

$$b_{k+1}^2=\|\mathbf{H}|k\rangle\|^2-a_k^2-b_k^2, \tag{43}$$

with $|-1\rangle\equiv 0$ and $b_0\equiv 0$. Thus, b_{k+1} may be interpreted as a normalization constant for $\mathbf{H}|k\rangle$ after it has been orthogonalized to $|k\rangle$ and $|k-1\rangle$, making $\langle k+1|k+1\rangle\equiv 1$. Once $\mathbf{H}$ is in tridiagonal form it is an easy task to obtain $G_{00}(u)$ and from it the susceptibility

$$\chi(u)=-\frac{1}{4\pi}[1/(u-a_0-b_1^2/\{u-a_1-b_2^2/[u-a_2$$
$$-b_3^2/(u-a_3-\ldots)]\})] \tag{44}$$

and the spectral function

$$g(s)=-\frac{1}{\pi}\mathrm{Im}[1/(s^+-a_0-b_1^2/\{s^+-a_1$$
$$-b_2^2/[s^+-a_2-b_3^2/(s^+-a_3-\ldots)]\})] \tag{45}$$

through continued fractions.

The evaluation of the Haydock coefficients a_k and b_k requires repeated applications of the matrix $\mathbf{H}$, each of which

takes of the order of $O(N^2)$ steps due to the long range of the dipolar interactions **T**. However, the computation may become feasible even for very large systems if we follow the steps that took us from Eq. (9) to Eq. (13). That is, we employ the hierarchical view of the aggregate and extend the space of dipolar configurations from $3N$ dimensions to $3(2N-1)$ by adding a coordinate corresponding to the dipole moments of each of the groups in the hierarchy, we replace $\mathbf{E}^{\mathrm{ex}}$ by $(\mathbf{E}^{\mathrm{ex}})'$ as in Eq. (11), and we replace **H** by $\mathbf{H}''$, in a similar fashion as the transformation from **M** to $\mathbf{M}''$ in Eq. (13), i.e., by replacing the N_ζ particle-particle interactions t_{ij}, $j \in \zeta$ by a single particle-group interaction $t_{i\zeta}$ whenever it is possible. Additional gains can be obtained in the evaluation of Eqs. (42) and (43) by replacing the $N_\zeta N_\xi$ particle-particle interactions t_{ij}, $i \in \zeta$, $j \in \xi$ by a single group-group interaction $t_{\zeta\xi}$ if the two groups are sufficiently small and far away. The speed and memory usage gains are very substantial.[31] For very large systems, the continued fractions in Eqs. (44) and (45) may sometimes be truncated, replacing their tail by a suitable terminator that accounts approximately for the remaining coefficients,[43] therefore introducing additional computational speedups.

III. RESULTS: SCALAR MODEL

In this section we apply the hierarchical methods presented above to the calculation of the optical properties of an ensemble of large fractal colloidal aggregates. In order to simplify the discussion of the results we present results for DLCA clusters embedded in a two-dimensional (2D) plane and illuminated in the direction normal to the plane, so that the external field is taken as position independent within the aggregate. Furthermore, we ignore the vectorial character of $\vec{p}$ and thus work within a scalar approximation. This could be physically realized if the induced dipole moments were perpendicular to the plane containing the aggregate, corresponding to a longitudinal excitation. Consistent with this, we will assume a nonretarded dipolar interaction $t_{ij} = -1/r_{ij}^3$. Thus, instead of calculating the scattering of light by the aggregate, in this section we calculate the Fourier transform of the spatial correlation function of the dipole moments induced in the system, closely related to the *dynamic form factor*[19,20] of the system. Nevertheless, to facilitate the comparison with the full vectorial calculation of the next section, we will employ the language of light scattering to discuss the results of this section. In Sec. IV we present results of a full vectorial calculations which confirm that the scaling properties of the longitudinally induced dipoles we obtain below do correspond qualitatively to those of the transverse dipoles, and that our results are useful to understand the nature of scaling for the problem of light scattering. It has been shown that the scalar approximation above yields qualitatively correct results in a context similar to the present one.[20]

A. Normal modes

We have employed the hierarchical representation for simulating the growth of colloidal aggregates in different regimes.[31] In Fig. 3 we illustrate the geometry of a DLCA cluster grown in two dimensions. Notice its branching structure with cavities and protuberances of all lengthscales, corresponding to a fractal of dimension $d_f \approx 1.45$. We remark that as our clusters were grown on a continuum and not on a discrete lattice,[19,20] avoiding thus artifacts which may arise from having only a small number of short range geometric configurations. In Fig. 4 we present the spectral density function $g(s)$ for an ensemble of 30 DLCA-2D clusters with 10^4 particles each, calculated using Eq. (45) and the hierarchical representation. There is a single band of normal modes extending from $s \approx 0.25$ to $s \approx 0.5$ which peaks at $s \approx 0.48$. The fine scale structure visible in Fig. 4 is not removed through ensemble averaging.

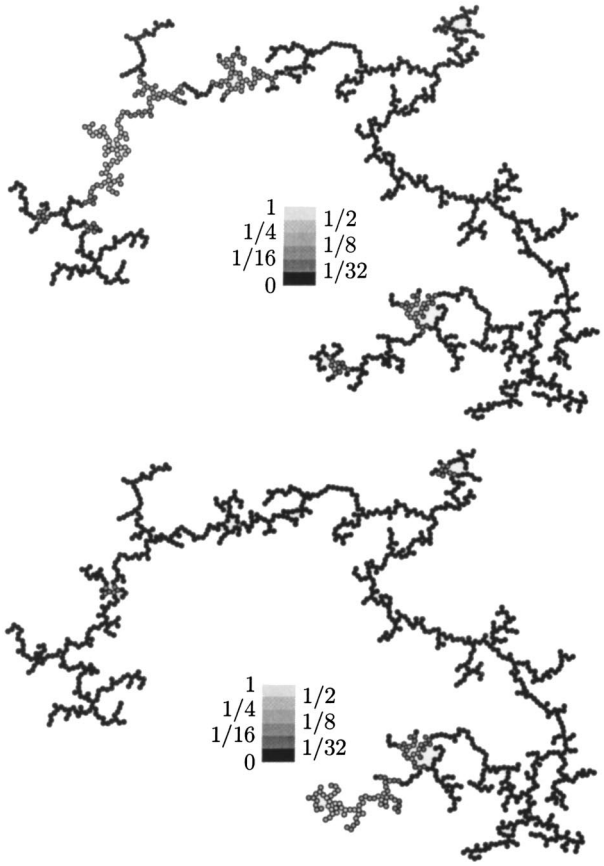

FIG. 3. Small $N = 10^3$ DLCA-2D aggregate with the normalized dipole moments $p/p_{\max}$ induced by an external field displayed in shades of gray. The upper panel corresponds to a normal mode with spectral variable $s = 0.4865$. The following normal mode corresponding to $s = 0.4887$ is shown in the lower panel. A small imaginary part $i\Gamma = 10^{-4} i$ was added to s.

To understand the nature of the modes, we have solved Eq. (13) hierarchically to obtain the induced dipoles p_i for different values of the spectral variable s. Figure 3 illustrates the induced dipole moment for two normal modes with values of s close to the peak of $g(s)$ for a particular rather small cluster. We notice that the local field is very strong on just a few particles. Thus, in the upper panel of Fig. 3, corresponding to $s = 0.4865$, only those particles in a small region close to the upper-left corner have an appreciable electric polariza-

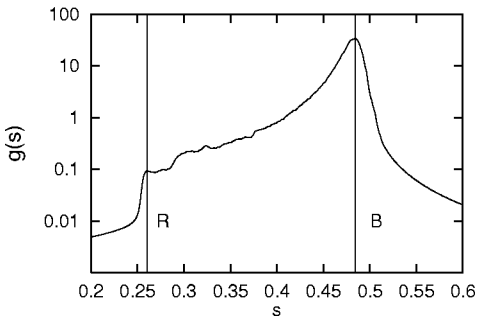

FIG. 4. Spectral density function $g(s)$ for an ensemble of 30 DLCA-2D aggregates with 10^4 particles each. To obtain a continuous curve, each mode was given a finite width $\Gamma = 10^{-3}$. *Red* (R) and *blue* (B) regions are indicated for later reference.

tion. These strongly polarized regions have been noticed before and have been referred to as *hot spots*.[18,44] The confinement of the field to such small regions when the frequency is tuned to a resonance of the fractal produces a field enhancement that may be observed through an amplification of nonlinear optical effects such as harmonic generation. Modifying the frequency by very small amounts produces dramatic redistributions of the dipole moments.[18–20] The lower panel of Fig. 3 illustrates how the hot spot at the upper-left corner disappears and a new hot spot appears close to the bottom of the system when the spectral variable increases by a very small amount up to the next resonance of the aggregate, at $s = 0.4887$. The long range phase correlation among simultaneously excited hot spots have been studied in detail for dipolarly interacting DLCA-3D clusters and for homogeneous random systems in the stationary[19,20] and the transient regimes,[45] as well as for planar random systems,[26] and interesting applications for ultrafast control of electromagnetic energy in ultrasmall spatial regions have been suggested.[46]

A close analysis of the hot spots shows that for values of s within a given spectral region, the local geometry of the excited area is similar. For example, in both panels of Fig. 3 the maximum dipole is attained at some group of four particles forming a small square. The particular square excited in the upper panel is far away from that excited in the lower panel, but its local geometry is similar. Within other spectral regions, the local geometry of the hot spots is different, and the response may be concentrated, for example, at relatively low density regions resembling a linear chain or at branching points resembling a letter *Y*. Thus, the local geometry of a given small subaggregate, not its position, determines the spectral region at which it resonates, thus becoming a hot spot, but the interactions with particles that are farther away within the large aggregate determine the precise frequency of the resonance.

Besides the local geometry, the hot spots also have characteristic phase relationships at different regions of the spectrum. In Fig. 5 we present details of the hot spots for two different frequencies. At the blue end (B) of the spectrum all of the dipole moments are in phase with each other, reminiscent of a ferromagnetic (F) ordering, while at the red end (R) of the spectrum, nearest neighbor dipoles at the hot spot alternate in sign, reminiscent of an antiferromagnetic (AF) ordering. This behavior is simply understood, as the field produced by any particle acts over the other particles in the direction opposite to its own dipole. Let us consider the simple case of only two interacting polarizable particles subject to harmonic internal forces (Fig. 6) lying on a plane and with their dipole moment normal to the plane. When the two dipoles are parallel, the field produced by one of them opposes the dipole moment of the other one, as if the restoring springs were stiffened and therefore increased their resonance frequency. On the other hand, when the dipoles are anti-parallel, the field produced by one of them would reinforce the dipole moment of the other one, as if the springs were softened and decreased their resonance frequency. The identification of the blue or red shift of a resonance with respect to the nominal resonance of an isolated sphere at $s = 1/3$ with a F or AF-like short range order at the hot spot is not possible when the dipoles lie on the plane of the aggregate nor when the aggregate is not planar, as the mutual effect of neighbor dipoles would depend not only on their relative direction, but also on their relative positions. This is one of the reasons for studying our simplified scalar model first.

According to the discussion above, the normal mode with the largest blueshift would correspond to an F excitation at a dense region. In Fig. 7 we show a few small isolated clusters. The F resonance for a close packed hexagon is at $s \approx 0.50$, close to the B end of the spectrum shown in Fig. 4. The close packed cluster does not support an AF mode due to the frustration inherent in the triangular lattice. However, an AF mode would be expected if the particles are located at sites of a square lattice. The rectangle shown in Fig. 7 has an AF resonance at $s \approx 0.25$, close to the R end of the spectrum.

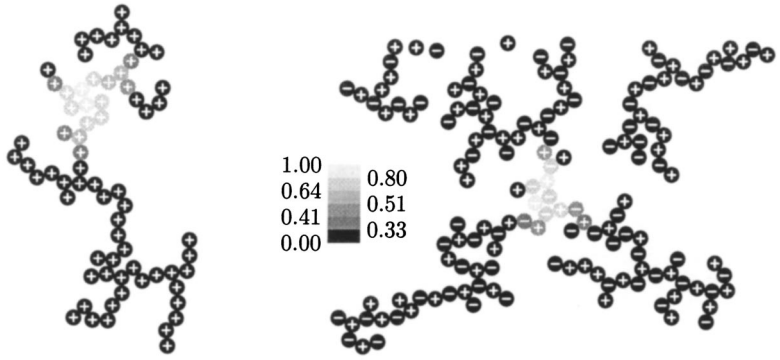

FIG. 5. Hot spot details for resonances close to the blue end (B) of the spectrum ($s = 0.4887$ (rotated with respect to Fig. 3), left panel) and close to the red end (R) of the spectrum ($s = 0.2527$, right panel). The shades of gray indicate the magnitudes of the dipole moments, while the signs indicate their relative phase. The scale of gray tones corresponds to successive powers of 0.8.

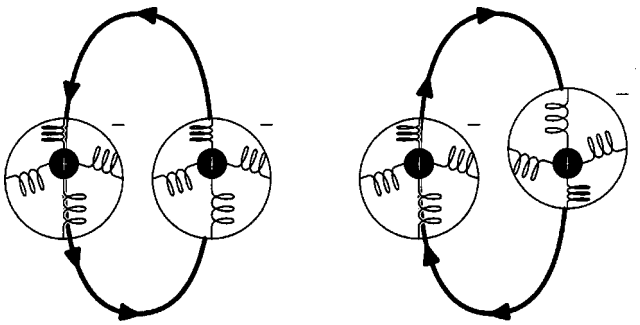

FIG. 6. Model polarizable particles made up of a negative shell bound by an harmonic restoring force to a positive fixed nucleus. The field produced by the particle at the right acting on the particle at the left is indicated by thick arrows. The left (right) panel shows that their mutual interaction increases (decreases) the restoring force when the dipoles are parallel (antiparallel).

Notice the similarity of this cluster to the local geometry of the hot spot shown in the right panel of Fig. 5. We also show in Fig. 7 an antisymmetric mode for a small square, whose resonance is at $s \approx 0.32$, corresponding to a peak in the spectra. Similarly, the symmetric and antisymmetric modes of a two particle chain resonate at $s \approx 0.38$ and 0.29, where the spectrum shows a small step and a conspicuous hump respectively, and the AF mode of a four particle Y structure, common at branching points of the aggregate, is at $s = 0.27$, where the spectra shows a tiny but still noticeable peak. Although they are not conclusive, this examples suggest that the abundant small scale structures seen in Fig. 4 may originate from the discrete resonances of small regions with characteristic geometries, which are somewhat shifted through their interactions with the rest of the aggregate.

According to Eq. (30), the spectral density function is a measure of the energy absorbed by the system. As the dipole moments alternate in sign at the R resonances, the total coupling to the external field is suppressed and $g(s)$ becomes about two orders of magnitude smaller than at the B resonances.

Figures 3 and 5 suggest that the dipolar resonances of an aggregate are localized.[18,44,47] Attempts have been made to characterize the localization of dipolar excitations in fractals through a localization length $L^{(q)}$, related to the qth moment of the spatial distribution of the dipole moments.[23,48] The resulting length depends on the choice of the particular moment q. It has been found that small changes of the spectral variable produce violent fluctuations[48] of $L^{(q)}$, so that a single localization length becomes insufficient for characterizing the system, requiring instead a distribution of localization lengths.[19] This behavior is refered to as *inhomogeneous localization* and is due to the possibility of simultaneous excitation of spatially separated hot spots due to the long range of the interaction. Actually, systems with long range nondipolar interactions present a similar behavior.[26]

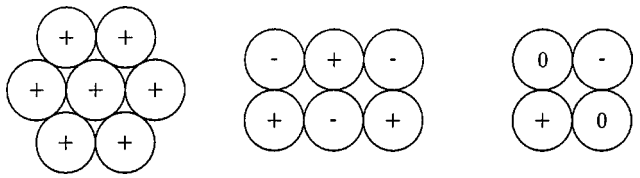

FIG. 7. Small isolated clusters with normal modes close to features of the spectrum shown in Fig. 4. The left panel shows an hexagonal close packed cluster with a ferromagneticlike mode at $s \approx 0.50$. The center panel shows a rectangular cluster with an antiferromagneticlike resonance at $s \approx 0.24$. The right panel shows an antisymmetric mode for a square cluster, with a resonance at $s \approx 0.32$.

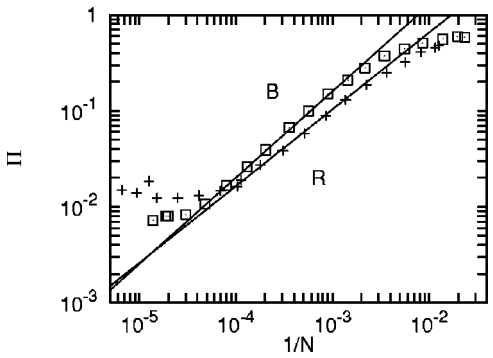

FIG. 8. Participation ratio Π averaged over an ensemble of 10^4 particle aggregates for different sized disks centered at the maxima of the induced dipolar moment of each aggregate, as a function of the number N of particles within the disk, for normal modes at $s \approx 0.485$ (squares) and $s \approx 0.260$ (crosses), close to the blue (B) and red (R) ends of the spectrum. An imaginary part $i\Gamma = 10^{-4} i$ was added to s. The straight lines correspond to the power law (47) with $\beta = 0.9$ (B) and $\beta = 0.8$ (R).

An alternative characterization of localization is through the participation ratio[49]

$$\Pi \equiv \left\langle \frac{\left(\sum_i p_i^2 \right)^2}{N \sum_i p_i^4} \right\rangle . \tag{46}$$

$\Pi \in [0,1]$ is a measure of the relative number of particles that participates in the excitation, independently of their position, making Π better behaved than the localization length for our system. As the number of particles N of the system increases, the participation ratio would go to zero as $\Pi \propto 1/N$ if the excitations were exponentially localized around the hot spots, even when several spatially separated hot spots are excited simultaneously. On the other hand, if the excitations were extended and the hot spots were but fluctuations over an otherwise constant background response, Π would become constant asymptotically. Fig. 8 shows that for our system the participation ratio obeys a power law

$$\Pi \propto N^{-\beta} \tag{47}$$

over a couple of decades, where $\beta \approx 0.9$ at B and $\beta \approx 0.8$ at R. Thus, it seems that the normal modes are not exponentially localized nor extended.[19] The observation of Anderson localization of light is still an open question.[50] The precise nature of the dipolar eigenstates in fractals and, more generally, within disordered systems with long ranged interactions should be further investigated.[26]

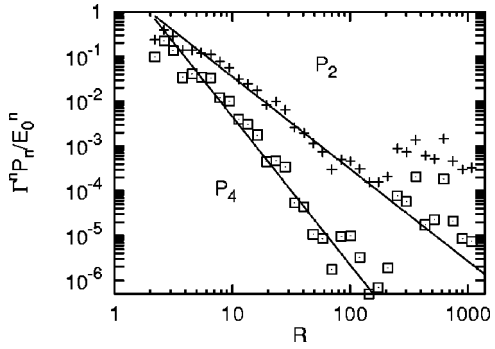

FIG. 9. Powers of the dipole moments $P_n(R)$ $(n=2,4)$, averaged over all particles within annular regions a of radii $0.9R$ and $1.1R$, centered at a hot spot and ensemble averaged, for normal modes close to $s=0.485$. An imaginary part $i\Gamma=10^{-4}i$ was added to s and the results were normalized to Γ^n/E_0^n.

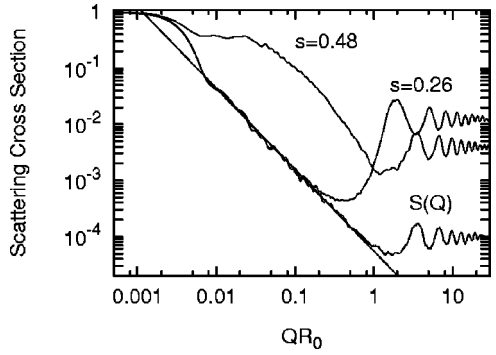

FIG. 10. Angularly and ensemble averaged normalized scattering cross section $\langle d\sigma(Q)/d\Omega\rangle/\langle d\sigma(0)/d\Omega\rangle$ as a function of the normalized scattering wave vector QR_0 for $N=10^4$ DLCA-2D aggregates. We display results for $s=0.26$ and $s=0.48$, close to R and B, respectively. An imaginary part $i\Gamma=10^{-4}i$ was added to s. We also show the structure factor $S(Q)/S(0)$ and the power law Q^{-d_f}.

As the value of β found above is close to the value expected for exponential localization, $\beta=1$, we look more closely at the decay of the excitation as we move away from the hot spots. Figure 9 displays the dependence of the ensemble averaged powers of the induced dipoles,

$$P_n(R)\equiv\left\langle \frac{\sum_i p_i^n \delta(R-r_i)}{\sum_i \delta(R-r_i)} \right\rangle \quad (n=2,4), \tag{48}$$

on the distance R to the largest dipole, calculated close to the blue end of the spectrum. Notice that over a range of lengthscales of about a decade, we can approximate

$$P_n \propto R^{-\alpha_n}, \tag{49}$$

where $\alpha_2\approx 2.06$ and $\alpha_4\approx 3.31$. We remark that $\alpha_4<2\alpha_2$, showing that $P_4(R)$ decays much more slowly than $P_2^2(R)$ and is therefore dominated by the large fluctuations of p_i. For a disk of large radius R containing $N\propto R^{d_f}$ particles, we would expect the averaged sum

$$\left\langle \sum_{r_i<R} p_i^n \right\rangle \propto \int_{R_m}^{R} R'dR' C(R')(R')^{-\alpha_n} \propto R^{d_f-\alpha_n} - R_m^{d_f-\alpha_n}, \tag{50}$$

where R_m is a small distance, of the order of R_0. As $\alpha_n > d_f$, this sum would become constant for large disks $R\to\infty$, and the participation ration would decay asymptotically as $\Pi\to 1/N$, although the decay is given by a power law and is not exponential. However, this regime is not reached in Fig. 8 as our calculation was done on finite samples and the power law (49) is violated[20] for large R, as seen in Fig. 9. The reason for the change in the behavior of $P_n(R)$ away from a decaying power law will be discussed below.

B. Scattering and scaling

As shown in Eqs. (17), (18), and (19), the differential section for light scattering is related to the Fourier representation $\vec{D}^{\perp}(\vec{Q})$ of the transverse projection of the dipole moments $\vec{p}_i$ induced within the system. Although our calculation was done within a scalar framework, for notational convenience we will employ scalar equations analogous to Eqs. (17)–(19) and discuss the scaling properties of $\langle|D(\vec{Q})|^2\rangle$ as if it were a differential scattering cross section. In Fig. 10 we show the ensemble and angular averaged values of the fictitious $\langle d\sigma/d\Omega\rangle$ for $N=10^4$ particle clusters for values of s close to B and R. For comparison, we also show the geometrical structure factor $S(Q)\propto\langle\Sigma_{ij}e^{i\vec{Q}\cdot\vec{r}_{ij}}\rangle$, which would be proportional to $\langle d\sigma/d\Omega\rangle$ in the absence of multiple scattering, and the power law Q^{-d_f} characteristic of a mathematical infinite fractal.

As expected, we find that $S(Q)$ is a scaling function proportional to Q^{-d_f} in a region $Q_{\min}<Q<Q_{\max}$, bounded on one side by $Q_{\min}\sim 1/R_M$ where R_M is the total size of the system ($Q_{\min}\approx 0.0075$ and $R_M\approx 1000R_0$ for our 10^4 particle aggregates) and on the other side by $Q_{\max}\sim 1/R_0$. The whole system behaves as a point polarizable particle when sampled with small wave vectors $Q<Q_{\min}$. Thus, $S(Q)$ becomes constant in the $Q\to 0$ limit. The finite size R_M of the system is also manifest for Q within the scaling region, where it produces small but observable oscillations in $S(Q)$. When sampled with very large wave vectors $Q>Q_{\max}$, an oscillatory structure due to the interference between the field scattered by nearest neighbor particles appears. In Fig. 10 this structure was calculated as if the particles were pointlike. Otherwise, we would have had to convolute the form factor of the individual particles into $S(\vec{Q})$. Consistency with the long-wavelength approximation would actually make the region $Q>1/R_0$ inaccessible. However, it is instructive to ignore this restriction and to explore the calculated $\langle d\sigma/d\Omega\rangle$ even for such large wave vectors. The shape of $S(Q)$ for large Q and the position of its maxima and minima are well reproduced by the average contribution $\langle 1+\cos[2QR_0\cos(\theta)]\rangle$ of a single dimer made up of two particles a distance $2R_0$ apart and oriented at a random angle θ with respect to the scattering wave vector $\vec{Q}$, as most of the particles in the aggregate form part of zigzagging linear

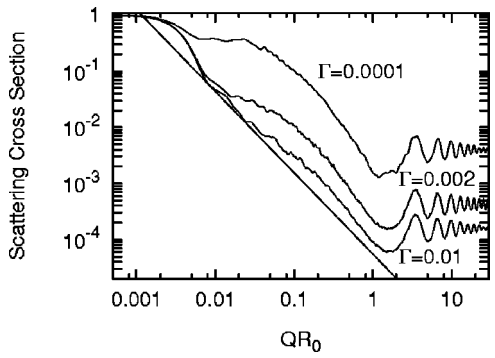

FIG. 11. Angularly and ensemble averaged normalized scattering cross section $\langle d\sigma(Q)/d\Omega\rangle/\langle d\sigma(0)/d\Omega\rangle$ calculated for normal modes at $s\approx 0.48$, close to B for $N=10^4$ DLCA-2D aggregates. We display results for three different values of $\Gamma=10^{-4}$,2 $\times 10^{-3}$,10^{-2}. The power law Q^{-d_f} is drawn as a reference.

chains with random orientations. The result is proportional to $1+j_0(2QR_0)$ where j_0 is the 0-th order Bessel function of the first kind.

The scattering cross section calculated for $s\approx 0.26$ is seen in Fig. 10 to scale as Q^{-d_f} within a region somewhat smaller than that for $S(Q)$. For small Q, $\langle d\sigma/d\Omega\rangle$ is indistinguishable from $S(Q)$, while for $QR_0>1$ the oscillations are out of phase with the oscillations of $S(Q)$. This confirms our previous remark that nearby particles tend to polarize in antiparallel directions when the excitation frequency lies close to the red end of the spectrum. On the other hand, for $s\approx 0.48$ the large Q oscillations are in phase with those of $S(Q)$, as the dipoles induced in nearby particles point in the same direction. Finally, we notice that at the blue end of the spectrum $\langle d\sigma/d\Omega\rangle$ does not seem to scale with the fractal dimension at all. In this case, Fig. 10 shows that the scattering cross section presents a wide shoulder which, if linearized within small regions, would yield power laws with exponents which differ from the fractal dimension. This suggests that scaling of the scattering cross section under resonance conditions is only approximate and that the scaling exponents depend on the frequency of the incoming light and therefore, they should not be naively linked to the geometrical fractal dimension.[17,51] These results are similar to the spectral dependence of the *dynamic form factor* found in Refs. 19 and 20.

In Sec. III A we found that at each spectral region the hot spots had a particular local geometry. Since the whole aggregate is scale invariant, we would expect that the set of subregions with a particular local geometry would constitute by itself a scale invariant fractal with the same dimension as the original aggregate. For example, the set of tips, with coordination number 1, or the set of branching points with coordination number 3, are fractals statistically similar to the whole aggregate. Thus, it could reasonably be expected that the set of hot points at a given frequency should form a fractal with dimension d_f and that therefore $\langle d\sigma/d\Omega\rangle$ should have scaled as Q^{-d_f}, independently of the scattering regime. This conclusion seems to contradict the numerical results displayed in Fig. 10. This inconsistency could be solved if the hot spots for each value of the spectral variable s were so diluted that at most, only a handful of them were present at a time within the finite aggregates on which we performed our simulations. To test this idea, we have to inquire into the typical distance between hot spots. As also discussed in Sec. III A, the exact frequency at which a given location resonates depends not only on its local geometry, but also on its environment. As there are no two regions with exactly the same global environment, it is conceivable that when the spectral variable s is given a well defined real value, at most a few isolated hot spots are excited. However, in our calculations above we have added a small imaginary contribution $i\Gamma$ to s. This is equivalent to giving a finite width $\Delta s\approx\Gamma$ to each of the normal modes, allowing them to overlap nearby resonances. Thus, the number of excited hot spots would depend on Γ and on the size of the system, and we expect that for a large enough system, or for a large enough dissipation, scaling with the exponent d_f should be recovered.

In Fig. 11 we present $\langle d\sigma/d\Omega\rangle$ calculated at B for different values of Γ. Clearly, as Γ increases, the scattering cross section approaches a scaling behavior. Figure 12 shows the module $|p_i|$ of the local dipole moments induced in a chosen aggregate. The left panel shows that when Γ is small the response is appreciable at only a few sites, and therefore no scaling is possible. As Γ increases the maximum value of the induced dipoles decrease and more peaks become visible, as shown in the right panel. Thus, if Γ is large enough, or if the system is large enough, the excited particles form themselves a fractal with the same dimension d_f as the aggregate and scaling is attained, as illustrated in Fig. 11.

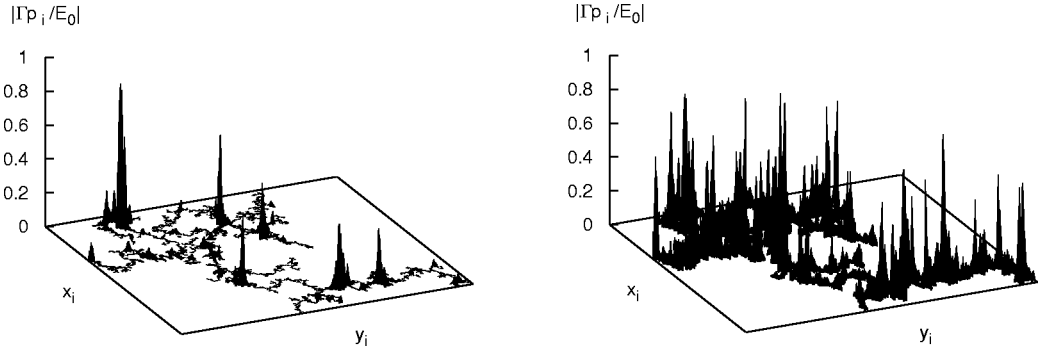

FIG. 12. Normalized magnitude of the induced dipole moments $p_i\equiv p(\vec{r}_i)$ for a $N=10^4$ DLCA-2D aggregate excited at $s\approx 0.48$, close to B. The left panel corresponds to $\Gamma=10^{-4}$ and the right panel corresponds to $\Gamma=2\times 10^{-3}$.

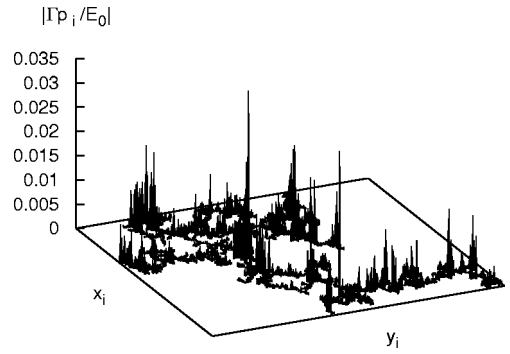

FIG. 13. Normalized magnitude of p_i as in Fig. 12 but for $s \approx 0.26$, close to R, with $\Gamma = 10^{-4}$.

Figure 13 shows the corresponding results for $s \approx 0.26$, close to R. We notice that the magnitude of the induced dipoles is much smaller than that corresponding to B, shown in the left panel of Fig. 12. This is due to the AF-like nature of the R normal modes; the coupling of a given dipole to the external field is nearly canceled by the coupling of its nearest neighbors, which tend to be in antiphase. For the same reason, the total dipole moment of any large area is small and its influence on the resonance frequency of far away hot spots becomes negligible. Thus, the distribution of excited hot spots for a given s at the red end of the spectrum is quite homogeneous, even for relatively small values of Γ. It is for these reasons that scaling is apparent in Fig. 10 at R but not at B.

As $g(s)$ may be interpreted as a projected normalized density of states, the number of excited hot spots N_h can be estimated as the number of normal modes,

$$N_h \approx N g \Gamma, \tag{51}$$

that fall within the width $\Delta s \approx \Gamma$ of each individual resonance s_n. As we argued above, we expect that in a large enough system, the hot spots form a fractal by themselves with the same dimension d_f as the aggregate. Thus, N_h should depend on the size R_M of the aggregate as

$$N_h(R_M) \propto \left(\frac{R_M}{L_h}\right)^{d_f}, \tag{52}$$

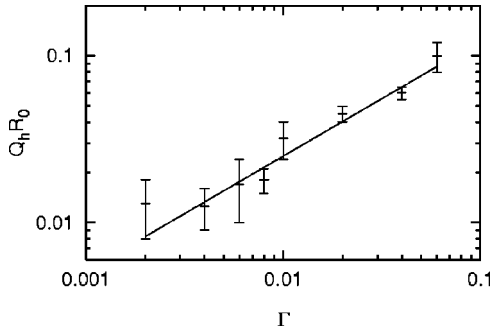

FIG. 14. Maximum scaling wave vector Q_h as a function of the linewidth Γ for resonances at $s \approx 0.48$, close to B. The straight line corresponds to Eq. (53). The error bars arise from the oscillations of $\langle d\sigma/d\Omega \rangle$ and are estimated subjectively.

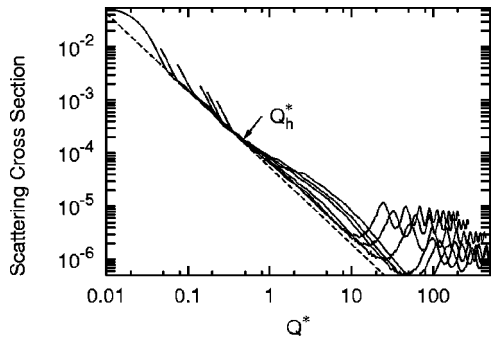

FIG. 15. Normalized averaged differential scattering cross section $\Gamma \langle d\sigma(Q)/d\Omega \rangle / \langle d\sigma(0)/d\Omega \rangle$ vs normalized scattering wave vector $Q^* \equiv Q R_0 / \Gamma^{1/d_f}$ evaluated at $s \approx 0.48$ close to B for different values of $\Gamma = 4 \times 10^{-3}$, 6×10^{-3}, 8×10^{-3}, 0.02, 0.04, and 0.06. For clarity, the curves are truncated beyond the left edge $Q^* < Q^*_{\min}(\Gamma)$ of the scaling region.

where we introduced the typical distance $L_h > R_0$ between neighboring induced dipole peaks. As the total number of particles in the fractal scales as $N(R_M) \propto (R_M/R_0)^{d_f}$, we can solve Eqs. (51) and (52) for L_h and write

$$Q_h R_0 \propto (g\Gamma)^{1/d_f}, \tag{53}$$

where $Q_h \equiv 1/L_h$. Notice that scaling of $\langle d\sigma/d\Omega \rangle$ as Q^{-d_f} can only be expected for wave vectors $Q < Q_h$ that are too small to sample the details of each individual hot spot. As scaling requires wave vectors $Q > Q_{\min}$ able to sample the innards of the system, no scaling at all may be obtained for finite systems of size $R_M < L_h$ smaller than the distance between hot spots. On the other hand, scaling is expected for large clusters of size $R_M \gg L_h$, and, in particular, it should always be present for infinitely large clusters independently of the linewidth Γ. These are the main results of the present paper. We have calculated the differential cross section for several values of Γ, as in Fig. 11, and we have identified approximately the wave vector Q_h that bounds the corresponding scaling region. The results are shown in Fig. 14. Although the precise identification of Q_h from Fig. 11 is difficult due to the oscillations originated in the finite size of the sample, leading to large errors, Fig. 14 is seen to be in good agreement with Eq. (53). Scaling of the scattering cross section with the fractal dimension within a region $Q_{\min} < Q < Q_h$ can be further demonstrated by plotting $\Gamma d\sigma/d\Omega$ as a function of the scaled wave vector $Q^* \equiv Q R_0 / \Gamma^{1/d_f}$. Figure 15 shows that curves for different values of Γ coalesce into one curve within a region $Q^*_{\min} < Q^* < Q^*_h$ where we identify $Q^*_h \approx 0.5$.

The existence of the lengthscale L_h also explains the behavior of $P_2(R)$ and $P_4(R)$, which, as shown in Fig. 9, decay as a power $R^{-\alpha_n}$ of the distance R to the main hot spot, but increases again for large R as other hot spots, at a distance $R \sim L_h$ are reached. Notice that the computation of a localization length in terms of the moments of the dipole moments induced in dissipative systems of a size R_M much larger than L_h would necessarily yield a result of the order of R_M due to the presence of many hot spots separated typically by the distance L_h. For systems of size $R_M \approx L_h$ the local-

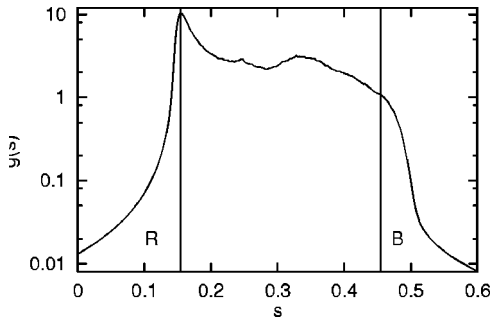

FIG. 16. Spectral density function $g(s)$ for an ensemble of 30 DLCA-2D aggregates with 10^4 particles each illuminated by a transverse electromagnetic wave propagating normal to the plane. Each mode was given a width $\Gamma = 2\times10^{-3}$. *Red* (R) and *Blue* (B) regions are indicated for later reference.

ization length is expected to vary wildly as some modes would have one hot spot and nearby modes might have a few separated hot spots simultaneously excited.[19]

IV. RESULTS: VECTORIAL MODEL

In Sec. III we presented results for a scalar model, corresponding to aggregates lying on a plane and excited by a field which points along the normal to the plane and whose value is constant along the plane, i.e., a longitudinal field. The ensuing longitudinal dipoles would be unable to radiate electromagnetic waves in the near forward direction, so that their Fourier transforms illustrated in Figs. 10 and 11 cannot be strictly interpreted in terms of differential light scattering cross sections. In this section we present results corresponding to a fully vectorial model, and we show that the main conclusions of the previous section are fit for the analysis of actual light scattering, notwithstanding the criticism above.

In Fig. 16 we show the spectral function $g(s)$ corresponding for the same 2D DLCA aggegates as on Sec. III, but illuminated by true transverse electromagnetic waves propagating in the direction normal to the plane of the aggregate. The spectral function differs considerably from that shown in

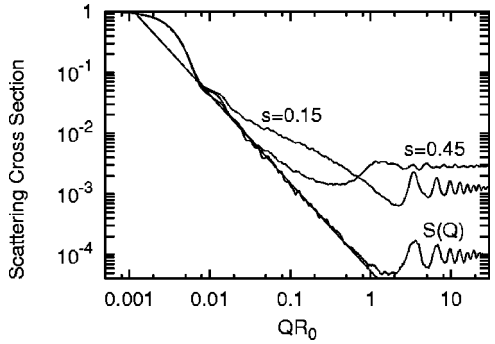

FIG. 17. Angularly and ensemble averaged normalized scattering cross section $\langle d\sigma(Q)/d\Omega\rangle/\langle d\sigma(0)/d\Omega\rangle$ as a function of the normalized scattering wave vector QR_0 for $N=10^4$ DLCA-2D aggregates illuminated with a transverse electromagnetic wave and with values of $s=0.15$ and 0.45, corresponding to the *red* (R) and *blue* (B) ends of the spectrum shown in Fig. 16 with an imaginary part $i\Gamma=0.002i$. As a reference, we also show the power law Q^{-d_f}.

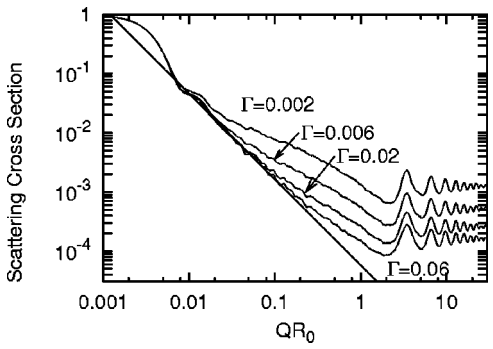

FIG. 18. Angularly and ensemble averaged normalized scattering cross section $\langle d\sigma(Q)/d\Omega\rangle/\langle d\sigma(0)/d\Omega\rangle$ calculated for normal modes at $s\approx0.15$, close to the left band edge of Fig. 16, for $N=10^4$ DLCA-2D aggregates excited by an in-plane field. We display results for three different values of $\Gamma=2\times10^{-3}$, 6×10^{-3}, 0.02, and 0.06. The power law Q^{-d_f} is drawn as a reference.

Fig. 4. The main peak is now redshifted with respect to the single particle resonance at $s=1/3$, the bandwidth is slightly larger, and the size of g(s) does not vary as much across the band as in Fig. 4. There are no simple explanations, as in Figs. 5–7, for the nature of each mode, as a couple of nearby dipoles in phase or in antiphase might reinforce or oppose each other, pushing the resonance frequency towards the red or towards the blue end of the spectrum depending on their relative positions, while in the scalar model they always induce a blueshift when in phase and a redshift when in antiphase.

In Fig. 17 we show the scattering cross sections corresponding to the same system as in Fig. 16 and for different values of *s*. As for the scalar model (Fig. 10), we found that there is scaling with the fractal dimension within regions which depend on the the spectral variable *s*. Close to the peak $s\approx0.15$ of $g(s)$ at the red (R) end of the spectrum, Fig. 17 shows no scaling with the fractal dimension d_f when $\Gamma=0.002$, although it might be argued that from $Q\approx0.02/R_0$ to $Q\approx0.3/R_0$ scaling is apparent with a smaller exponent. For large wave vectors there are oscillations in phase with those of the structure factor $S(Q)$, as in the scalar model at R. On the other hand, at $s=0.45$ and close to the blue (B) end, there is a small scaling region with exponent d_f extend-

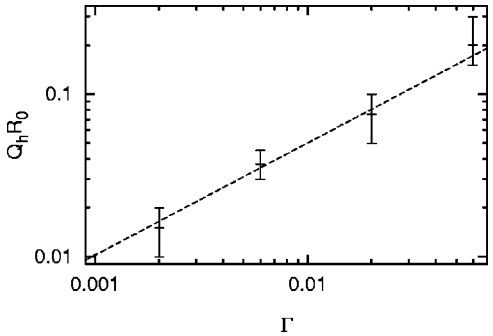

FIG. 19. Maximum scaling wave vector Q_h as a function of the linewidth Γ for resonances at $s\approx0.15$, close to the left band edge of Fig. 16, for $N=10^4$ DLCA-2D aggregates excited by an in-plane field. The straight line corresponds to Eq. (53).

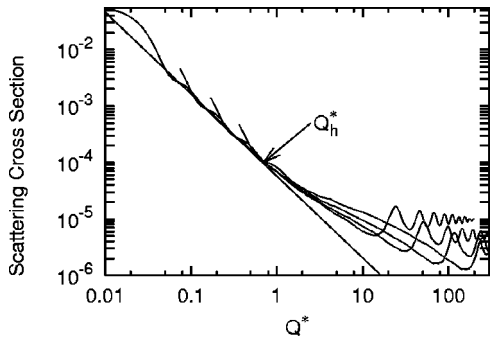

FIG. 20. Normalized averaged differential scattering cross section $\Gamma\langle d\sigma(Q)/d\Omega\rangle/\langle d\sigma(0)/d\Omega\rangle$ vs normalized scattering wave vector $Q^* \equiv QR_0/\Gamma^{1/d_f}$ evaluated at $s \approx 0.15$ close to R for different values of $\Gamma = 2\times10^{-3}$, 6×10^{-3}, 0.02, and 0.06. For clarity, the curves are truncated beyond the left edge $Q^* < Q^*_{\min}$ of the scaling region.

ing from from $Q_{\min} \approx 0.0075/R_0$ to $Q_h(0.45+0.002i) \approx 0.05/R_0$. Unlike the scalar model, there are small oscillations for large Q with twice the period of the oscillations of $S(Q)$, due to the presence of both F and AF tendencies along different directions. Furthermore, there is a peak at $QR_0 \approx 1$ suggesting oscillations in the dynamic form factor with a period $\approx 6R_0$, not unlike those reported in Refs. 19 and 20. For a fixed frequency, Fig. 18 shows that scaling depends on the dissipation parameter Γ and that the scaling range increases with Γ as in the scalar model. The dependence of Q_h on the dissipation parameter is shown in Fig. 19. Notice that $Q_h \propto \Gamma^{-1/d_f}$, thus confirming with a full vectorial calculation the results obtained in the previous section within a scalar model. Scaling within the region $Q_{\min}$–Q_h may be further demonstrated by multiplying the scattering cross section by Γ and plotting it as a function of the scaled wave vector Q^*. Figure 20 shows that, as in Fig. 15, curves corresponding to different values of Γ coalesce on top of each other within a region $Q^*_{\min}(\Gamma) < Q^* < Q^*_h$, where we identify $Q^*_h \approx 0.7$.

It has been reported that the scaling of the light scattered by aggregated aqueous Au colloids[16] may be removed by dilution,[17] but it has been further argued that if care is taken not to break the individual aggregates,[52] scaling remains even after dilution. These experimental results would be consistent with our calculations, if the typical size R_M of the aggregates was much larger than L_h only in the experiments where scaling was observed[16,52] but not in others.[17] Thus, an independent measurement of the size of the scatterers would be useful to settle the ensuing controversy.[51] It has been further observed that the scaling exponent depends on the wavelength. For instance, light scattered from three dimensional DLCA colloidal clusters made up of $R_0 \approx 8$ nm Au spheres was measured in Ref. 17 and scaling $d\sigma/d\Omega \propto Q^{-y}$ was obtained, but with an exponent $y \approx 1.78$ for $\lambda_1 \approx 457$ nm and with a different value $y = 1.64$ for $\lambda_2 \approx 632$ nm. We have performed full vectorial calculations[31] of the spectral density function $g(s)$ for DLCA-3D aggregates whose fractal dimension is $d_f \approx 1.8$ and we have found a band of normal modes that extends from $s \approx 0.15$ to 0.53. Fortunately, both wavelengths λ_1 and λ_2 correspond to similar values u' ≈ 0.15 of the real part of the spectral variable [Eq. (22)], close to the left edge of the band. Thus, from the imaginary parts $\Gamma = u''$ we may compare the corresponding lengths L_h employing Eq. (53). It turns out that L_h is about five times larger close to λ_2 than close to λ_1. Thus, it is possible to have clusters that are large enough so that their scattering cross sections scales with the fractal dimension close to λ_1 but at the same time so small that a different exponent or even no scaling is found at λ_2. This might explain the results of Ref. 17. Similarly, $u' \approx 0.18$ at $\lambda \approx 480$ nm for both Au and Ag particles in water. However, Γ is much larger for Au than for Ag at this wavelength, so that the minimum size required to ensure scaling with exponent d_f of the light scattered by Ag colloids turns out to be about 17 times larger than the corresponding size for Au colloids. Therefore, it is possible to grow Au colloids of such size that the light they scatter does scale with exponent d_f, while similarly grown Ag colloids of the same size and dimension show no such scaling.

V. CONCLUSION

We have developed and applied a multi-resolution binary-tree data representation and the corresponding hierarchical algorithms to calculate the dipole moments induced by an external field acting on an ensemble of large fractal aggregates. We calculated the Bergman spectral function $g(s)$ which accounts for the geometry of the system and may be employed to calculate its susceptibility for an arbitrary composition. For DLCA-2D clusters polarized in the direction normal to their embedding plane, and subject to long range nonretarded dipolar interactions, we obtained a band of normal modes that extends from $s \approx 0.25$ to 0.50 with a narrow peak at $s \approx 0.48$, where s is the spectral variable. For the same clusters but polarized along their embedding plane the band extends from $s \approx 0.14$ to 0.51 and is slightly peaked at $s \approx 0.15$.

We analyzed individual normal modes for polarization normal to the plane and for s at both ends of the spectrum. We found that the response was confined to small hot spots whose position varies wildly with s but whose local geometry is characteristic for each spectral region. At the *blue* end of the spectrum, the induced dipoles are arranged in a ferromagnetical fashion, while at the *red* end they are arranged antiferromagnetically. The spectral function displays a small-scale structure which may be related to the normal excitations of small subclusters with characteristic geometries. We inquired into the localization properties of the normal modes and found that the participation ratio Π tends to zero as the number of particles N increases, following a power law $N^{-\beta}$, where $\beta \approx 0.8$–0.9, according to the spectral region. Thus, the states are not extended nor localized in the usual sense. Further analysis showed that the averaged powers of the induced moments $P_n(R)$ $(n=2,4)$ decay as $R^{-\alpha_n}$, with $\alpha_2 \approx 2.06$ and $\alpha_4 \approx 3.31$. As it turns out that $\alpha_n > d_f$, we would have obtained $\beta = 1$ asymptotically, as for localized states, were it not for the appearance of a dissipation dependent lengthscale L_h which characterizes the typical distance between hot spots. We calculated the Fourier transform of the

dipolar distribution, and from it, the differential scattering cross section $\langle d\sigma/d\Omega \rangle$. We found that even under resonant conditions, $\langle d\sigma/d\Omega \rangle$ might scale as Q^{-d_f}, but only if the size of the system R_M is larger than the characteristic distance L_h among hot spots. Our use of the longitudinal dipoles induced by a longitudinal field lead to a simple interpretation of our results. We were thus able to understand the geometry of the hot spots at different spectral regions, the relative phase of the dipoles induced at nearby positions and the overall shape of the spectrum. Although not as easy to interpret, we verified that full vectorial calculations for DLCA-2D clusters excited by transverse electromagnetic waves yield similar results.

To simplify our calculations we made use of some approximations. As we neglected the multipolar interactions between nearest neighbor particles, our spectrum contains the resonances that arise from the $l=1$ surface plasmon of the individual spheres at $s=1/3$, but misses the resonances expected to arise from the $l>1$ surface plasmons[24,25] of each particle at $s=l/(2l+1)$. We expect multipolar corrections to the spectral function $g(s)$ when the colloidal particles actually touch each other, although these corrections may be minimized by coating the particles before aggregation. Nevertheless, we believe that our main result regarding the existence of a dissipation dependent length scale which determines the scaling region will prove robust. We also neglected retardation in the particle-particle interactions. As in our system, nearest neighbors actually touch each other, the nonretarded interactions between them are much stronger than the retarded interactions with faraway particles. Thus, we may separate the interparticle interactions into a strong nonretarded part and a small retarded correction that only becomes important at distances of the order of the wavelength. Our approach is thus equivalent to accounting for the nonretarded interaction through an infinite order multiple scattering calculation, while treating the corrections due to retardation within the first Born approximation. It has been shown[18] that, when applied to colloidal aggregates, this approach leads to negligible errors.

In conclusion, the differential cross section for the scattering of light does scale with the scattering wave vector Q as Q^{-d_f} even in the multiple scattering regime, but only for aggregates with a size R_M larger than the distance L_h between hot spots and for wave vectors that obey $Q_{\min}<Q<Q_h$, where $Q_{\min}\sim 1/R_M$ and $Q_h\sim 1/L_h$. The distance L_h depends on the real part u' of the spectral variable through the nature of the excited modes, and it decreases with their linewidth $u''=\Gamma$ as $L_h\propto\Gamma^{-1/d_f}$. Thus, for a given composition, L_h depends on the frequency of the exciting light ω through the dielectric functions of the particles $\epsilon(\omega)$ and of the host $\epsilon_h(\omega)$. It is then possible that the light scattered by a given aggregate scales with exponent d_f for certain wavelengths and does not scale or seem to scale with a different exponent for another wavelength. It is also possible that at some fixed wavelength, scattering from some aggregates scale with exponent d_f while scattering from aggregates with identical geometry but a different composition do not. This frequency, size, and composition dependent behavior might lie at the core of the ongoing controversy over scaling and its interpretation in the scattering of light by fractal aggregates under resonance conditions.[17,51–53]

ACKNOWLEDGMENTS

We acknowledge the support received from DGAPA-UNAM (Grants Nos. IN110999 and IN117402) and CIP-COMEX. We are grateful to François Leyvraz, Ronald Fuchs, and to Hernan Larralde for very illuminating discussions and to Catalina López-Bastidas for her useful suggestions.

*Electronic address: gortiz@fis.unam.mx
†Electronic address: mochan@fis.unam.mx

[1] B. B. Mandelbrot, *The Fractal Geometry of Nature* (Freeman, San Francisco, 1983).
[2] T. A. Witten and L. M. Sander, Phys. Rev. B **27**, 5686 (1983).
[3] P. Meakin, Phys. Rev. Lett. **51**, 1119 (1983).
[4] P. Meakin, Phys. Rev. A **27**, 604 (1983).
[5] W. D. Brown and R. C. Ball, J. Phys. A **18**, L517 (1985).
[6] J. Board and K. Schulten, Comput. Sci. Eng. **2**, 76 (2000).
[7] J. Barnes and P. Hut, Nature (London) **324**, 446 (1986).
[8] A. W. Appel, SIAM (Soc. Ind. Appl. Math.) J. Sci. Stat. Comput. **6**, 85 (1985).
[9] L. Greengard, Science (Washington, DC, U.S.) **265**, 909 (1994).
[10] P. Ossadnik, Physica A **176**, 454 (1991).
[11] D. A. Weitz and M. Oliveria, Phys. Rev. Lett. **52**, 1433 (1984).
[12] D. W. Schaefer, J. E. Martin, P. Wiltzius, and D. S. Cannell, Phys. Rev. Lett. **52**, 2371 (1984).
[13] J. Teixeira, in *On Growth and Form*, edited by H. E. Stanley and N. Ostrowsky (Martinus Nijhoff, Dordrecht, 1986), pp. 145–162.
[14] R. Amal, J. A. Raper, and T. D. Waite, J. Colloid Interface Sci. **140**, 158 (1990).
[15] M. L. Anderson, C. A. Morris, R. M. Stroud, C. I. Merzbacher, and D. R. Rolison, Langmuir **15**, 674 (1999).
[16] D. A. Weitz, J. S. Huang, M. Y. Lin, and J. Sung, Phys. Rev. Lett. **54**, 1416 (1985).
[17] J. P. Wilcoxon, J. E. Martin, and W. D. Schaefer, Phys. Rev. Lett. **58**, 1051 (1987).
[18] V. M. Shalaev, Phys. Rep. **272**, 61 (1996).
[19] M. I. Stockman, Phys. Rev. E **56**, 6494 (1997).
[20] M. I. Stockman, Phys. Rev. Lett. **79**, 4562 (1997).
[21] G. P. Ortiz and W. L. Mochán, in *Proceedings of SPIE*, edited by V. L. Brudny, S. A. Ledesma, and M. C. Marconi (SPIE, Bellingham, WA, 2001), Vol. 4419, pp. 752–755.
[22] F. Claro, Phys. Rev. B **30**, 4989 (1984).
[23] V. A. Markel, V. Shalaev, E. B. Stechel, W. Kim, and R.L. Armstrong, Phys. Rev. B **53**, 2425 (1996).
[24] R. Rojas and F. Claro, Phys. Rev. B **34**, 3730 (1986).
[25] R. Fuchs and F. Claro, Phys. Rev. B **39**, 3875 (1989).
[26] M. I. Stockman, S. V. Flaeev, and D. J. Bergman, Phys. Rev. Lett. **87**, 177401 (2001).
[27] J. Zhang and J. Buffle, J. Colloid Interface Sci. **174**, 500 (1995).
[28] D. Myers, *Surfaces, Interfaces, and Colloids*, 2nd ed. (Wiley, Toronto, 1999), Chap. 14.

[29] S. B. Singham and C. F. Bohren, Opt. Lett. **12**, 10 (1987).
[30] S. B. Singham and C. F. Bohren, J. Opt. Soc. Am. A **5**, 1867 (1988).
[31] G. P. Ortiz and W. L. Mochán, Physica B (to be published); G. P. Ortiz, Ph.D. thesis, State University of Morelos, México, 2003; G. P. Ortiz and W. L. Mochán (unpublished).
[32] *Compaq Extended Math Library Reference Guide*, Compaq Computer Corporation, Houston (1999).
[33] F. M. Gomes and D. C. Sorensen, *Arpack++ Reference Guide (Version 1.2)* (2000).
[34] F. Claro and R. Fuchs, Phys. Rev. B **44**, 4109 (1991).
[35] D. J. Bergman, Phys. Rep. **43**, 377 (1978).
[36] D. Stroud, G. W. Milton, and B. R. De, Phys. Rev. B **34**, 5145 (1986).
[37] R. G. Barrera and R. Fuchs, Phys. Rev. B **52**, 3256 (1995).
[38] R. Fuchs (personal communication).
[39] *The Recursion Methods and its Applications*, edited by D. G. Pettifor and D. L. Weaire (Springer-Verlag, Berlin, 1985).
[40] R. G. Barrera, C. I. Mendoza, and R. Fuchs, Physica B **279**, 29 (2000).
[41] C. I. Mendoza, Ph.D. thesis, National University of México, 1999.
[42] R. Haydock, Solid State Phys. **35**, 215 (1980).
[43] C. M. M. Nex, in *The Recursion Method and Its Applications*, edited by D. G. Pettifor and D. L. Weaire (Springer-Verlag, Berlin, 1985).
[44] V. A. Markel, V. M. Shalaev, P. Zhang, W. Huynh, L. Tay, T. L. Haslett, and M. Moskovits, Phys. Rev. B **59**, 10903 (1999).
[45] M. I. Stockman, Phys. Rev. Lett. **84**, 1011 (2000).
[46] M. I. Stockman, S. V. Flaeev, and D. J. Bergman, Phys. Rev. Lett. **88**, 067402 (2002).
[47] D. P. Tsai, J. Kovacs, Z. Wang, M. Moskovits, V. M. Shalaev, J. S. Suh, and R. Botet, Phys. Rev. Lett. **72**, 4149 (1994).
[48] M. I. Stockman, L. N. Pandey, and T. F. George, Phys. Rev. B **53**, 2183 (1996).
[49] J. T. Edwards and D. J. Thouless, J. Phys. C **5**, 807 (1972).
[50] M. C. W. van Rossum and T. M. Nieuwenhuizen, Rev. Mod. Phys. **71**, 313 (1999).
[51] J. P. Wilcoxon, J. E. Martin, and W. D. Schaefer, Phys. Rev. A **39**, 2675 (1989).
[52] D. A. Weitz, M. Y. Lin, H. M. Lindsay, and J. S. Huang, Phys. Rev. Lett. **58**, 1052 (1987).
[53] Z. Chen, P. Sheng, D. A. Weitz, H. M. Lindsay, M. Y. Lin, and P. Meakin, Phys. Rev. B **37**, 5232 (1988).